Xia et al. Protection and Control of Modern Power Systems (2018) 3:33
https://doi.org/10.1186/s41601-018-0109-x

Protection and Control of Modern Power Systems

ORIGINAL RESEARCH Open Access

A new ensemble-based classifier for IGBT open-circuit fault diagnosis in three-phase PWM converter

Yang Xia*, Bin Gou and Yan Xu

Abstract

Three-phase pulse width modulation converters using insulated gate bipolar transistors (IGBTs) have been widely used in industrial application. However, faults in IGBTs can severely affect the operation and safety of the power electronics equipment and loads. For ensuring system reliability, it is necessary to accurately detect IGBT faults accurately as soon as their occurrences. This paper proposes a diagnosis method based on data-driven theory. A novel randomized learning technology, namely extreme learning machine (ELM) is adopted into historical data learning. Ensemble classifier structure is used to improve diagnostic accuracy. Finally, time window is defined to illustrate the relevance between diagnostic accuracy and data sampling time. By this mean, an appropriate time window is achieved to guarantee a high accuracy with relatively short decision time. Compared to other traditional methods, ELM has a better classification performance. Simulation tests validate the proposed ELM ensemble diagnostic performance.

Keywords: IGBT open-circuit fault, Extreme learning machine (ELM), Data-driven method, Ensemble structure

1 Background

Nowadays, induction motor drive systems fed by three-phase pulse width modulation (PWM) converters have been widely used in industrial applications [1]. With the advance of power semiconductor technology, insulated gate bipolar transistors (IGBTs) are commonly used in such systems to adjust the output signal of the converters. However, according to the industrial statistics, 38% of the converter faults are caused by the failure of power device [2] [3]. Power devices faults in converter may result in unstable output voltage and frequency, and can lead to the shutdown of the drive system. Thus, fast and accurate fault diagnosis method for IGBT has attracted extensive attentions [4].

In general, IGBT faults can be categorized into open-circuit fault and short-circuit fault. Short-circuit fault is usually caused by over-voltage or overheating. In practice, short-circuit fault of IGBT is usually protected by standard protection system, such as fuse and disconnecting switch [5].As a result, the abnormal state caused by short-circuit, such as over-current, may only last a very short period. On the other hand, open-circuit fault usually results in sustained period of abnormal states and can significantly degrade the converter performance. For PWM converters, the open-circuit situation is more complex because of the existence of a number of IGBTs in a converter. When open-circuit fault occurs, it is necessary to quickly detect and locate the faulty IGBTs. Hence, this paper concentrates on IGBT open-circuit faults in three-phase PWM converters.

Diagnosis methods of IGBT faults can be categorized generally into model-based, signal-based, knowledge-based, hybrid and active methods [5]. For model-based method [6–11], models of industrial processes or systems are the foundation and have to be derived from physical principles or systems identification techniques. The measured outputs of system models are then compared with the predicted outputs and the consistency is evaluated to diagnose faults [5]. This requires a high-level understanding of the practical systems and the consideration of other environmental factors in the actual working situation. Therefore, model-based

* Correspondence: xiay0020@e.ntu.edu.sg
Electric Power Research Laboratory, School of Electrical and Electronic Engineering, Nanyang Technological University, S2.2 B7, 50 Nanyang Avenue, Singapore 639798, Singapore

method always requires tiresome and length tuning for an accurate. For signal-based methods [12–16], measured signals are used for the diagnostic process. Feature selection, such as RELIEFF [17], is a methodology to evaluate the quality of signal features according to their distinction among instance near each other and to select several top best features. Similarly, feature extraction is also an approach to decrease the signal dimension, such as the principle component analysis (PCA) [18]. This is achieved by transforming original datasets into a reduced set of features. The initial features are selected as a subset, which contains the relevant information from the input data. By those features, diagnostic algorithm can analyze symptoms to make a fault diagnosis decision. However, such signal-based methods require long processing time and the diagnostic performance is easily affected by fluctuation of loads.

Both model-based and signal-based methods require a prior knowledge on system models or signal patterns. Furthermore, signal-based method is easily influenced by load fluctuation, and this is a significant drawback in online application. Hence these methods are either sensitive to system load or with low detection speed. On the contrary, knowledge-based method [19–25] is based on large volumes of historical data [26] which can be obtained by simulations and experiments. The artificial intelligent technique can also be combined with data-driven methodology to extract the mapping relationship knowledge between the online input data and the diagnosis results according to the historical data. Thus, this method is also called a data-driven method.

In order to improve fault diagnosis, this paper develops a data-driven fault diagnosis method for PWM converter fed induction motor drive system. The inputs in the fault diagnosis scheme are three-phase currents and the outputs are fault types and location. Because load current is measured for the control algorithm of PWM converters, no additional sensors are required in the system. A novel learning network, namely extreme learning machine (ELM) [27] is applied to develop a diagnostic method for IGBT open-circuit faults. ELM is a randomized learning neural network, whose input weights and bias are randomly determined in ELM learning and the output weights are computed without traditional iteration. As a result, instead of lengthy training time, ELM has a fast learning speed which allows it to solve problems with large volumes of data. Due to its fast learning speed, ELM has already been used in detection of microgrid islanding events [28] and real-time dynamic security assessment of power systems [29]. However, this method has not been adopted in fault diagnosis of power electronics devices. To guarantee accuracy, the ensemble structure is adopted which contributes to increasing the robustness of diagnosis performance. In addition to improve learning process, the relevance between the time window width of signal sampling and diagnosis accuracy is analyzed to select the suitable time window. Thus, the diagnosis performance of the scheme can be significantly improved.

Through online application, it shows that due to the fast learning speed of ELM, the proposed scheme is feasible to identify IGBT open-circuit faults with balanced diagnostic accuracy and speed. The simulation also validates that the classification performance is independent of voltage ripple, and harmonics, speed and load fluctuations.

2 System description and fault analysis

2.1 Circuit topology of traction converter

The circuit topology of a two-level three-phase PWM converter is shown in Fig. 1. T_1, T_2...T_6 are IGBTs and D_1, D_2...D_6 are anti-parallel diodes. An induction motor is located at the load side represented by equivalent inductances of Z_a, Z_b and Z_c. i_a, i_b, i_c are three-phase currents of the converter and motor stator [30].

From Fig. 1, when the converter operates in normal working state, the sum of three-phase currents in traction motor's stator is zero, and so as the sum of three-phase voltage i.e.:

$$u_{an} + u_{bn} + u_{cn} = Z_a i_a + Z_b i_b + Z_c i_c = 0 \tag{1}$$

In (1), u_{an}, u_{bn}, u_{cn} are three phase output converter voltages. Based on Kirchhoff's voltage law, the following equations can be obtained:

$$\begin{cases} u_{an} = u_{ao} - u_{no} \\ u_{bn} = u_{bo} - u_{no} \\ u_{cn} = u_{co} - u_{no} \end{cases} \tag{2}$$

$$u_{no} = u_{an} + u_{bn} + u_{cn} = \frac{1}{3}(u_{ao} + u_{bo} + u_{co}). \tag{3}$$

Defining the switch function as:

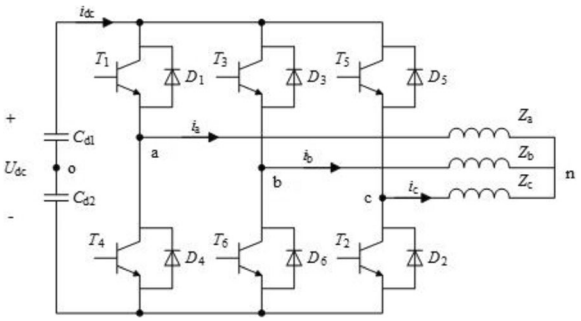

Fig. 1 The topology structure of drive system

$$S = \begin{cases} 1 & \text{the upper transistor is closed} \\ -1 & \text{the lower transistor is closed} \end{cases}'$$

The three-phase load voltage can be expressed by:

$$\begin{cases} u_{ao} = S_a \cdot \dfrac{U_{dc}}{2} \\ u_{bo} = S_b \cdot \dfrac{U_{dc}}{2} \\ u_{co} = S_c \cdot \dfrac{U_{dc}}{2} \end{cases} \quad (4)$$

Thus, the voltage between the DC middle point and the load neural point can be defined as:

$$u_{no} = \frac{U_{dc}}{6}(S_a + S_b + S_c). \quad (5)$$

Therefore, the calculation of the phase voltages of the load motor is defined as:

$$\begin{bmatrix} u_{an} \\ u_{bn} \\ u_{cn} \end{bmatrix} = \frac{U_{dc}}{6} \begin{bmatrix} 2 & -1 & -1 \\ -1 & 2 & -1 \\ -1 & -1 & 2 \end{bmatrix} \begin{bmatrix} S_a \\ S_b \\ S_c \end{bmatrix} \quad (6)$$

2.2 IGBT open-circuit fault analysis

Upper arm fault - when the upper switch is in open-circuit fault (e.g. T_1), the DC bus current i_{dc} cannot flow through T_1. Considering the stator winding of the traction motor is in star connection and without grounded neural, the sum of the three-phase currents remains at zero. Hence, i_a becomes negative, whereas i_b and i_c will be added with positive DC components. By introducing the open-circuit fault, the waveforms of three-phase currents are distorted and become asymmetric as shown in Fig. 2. The output electromagnetic torque of the traction motor is reduced and oscillates severely, which is harmful for system security and stability.

Lower arm fault - the fault phenomenon when the lower switch is under open-circuit fault (e.g. T_4) is similar to the previous case. When T_4 is in open-circuit fault, i_{dc} cannot feed the load through T_4. Thus, current in phase A becomes positive, and i_b and i_c contain negative DC components. The waveform become distorted as depicted in Fig. 3.

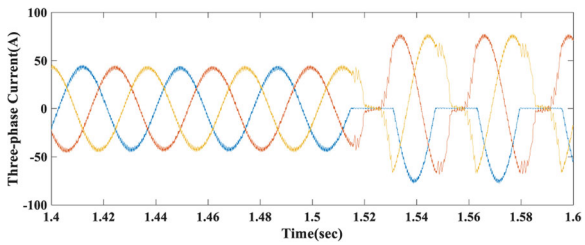

Fig. 2 The waveform when T_1 is under open-circuit fault

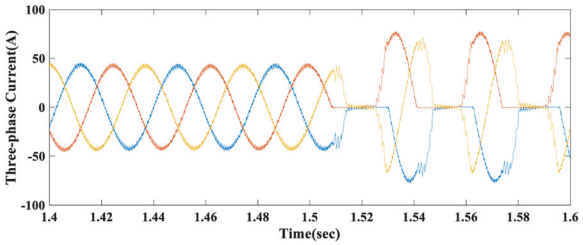

Fig. 3 The waveform when T_4 is under open-circuit fault

Both upper and lower arms fault – when both arms in the same phase (e.g. T_1, T_4) are open-circuit, the DC bus current i_{dc} only flows to the traction motor through phase C and B. Hence, current in phase A becomes zero, and stator currents in phase B and C have opposite values as depicted in Fig. 4.

2.3 Fault labeling for converter

To identify the fault type and location, 6 fault types of single IGBT open-circuit, 15 fault types of double IGBT open-circuit and a normal working condition are defined in this paper according to different status of the converter, which are summarized in Table 1:

3 Extreme learning machine

3.1 ELM structure

ELM is a novel randomized neural network [27] and Fig. 5 shows its structure. As a general single-hidden layer feed-forward neural network (SLFN), ELM consists of three layers: the input layer, hidden layer and output layer.

For a training set $\{(\boldsymbol{x}_i, \boldsymbol{d}_i)|\boldsymbol{x}_i \in R^J, \boldsymbol{d}_i \in R^K\}_{i=1}^{L}$, where L is the number of sample, $\boldsymbol{x}_i = [x_{i1},\ldots,x_{ij}]$ is the input vector with J features and $\boldsymbol{d}_i = [d_{i1},\ldots,d_{iK}]$ is the desired output vector with K features.

The relationship between the actual output vector $\boldsymbol{t}_i = [t_{i1},\ldots,t_{iK}]$ and $\boldsymbol{x}_i$ is shown:

$$\boldsymbol{h}_i = g(\boldsymbol{w}_{IH}\boldsymbol{x}_i) \quad (7)$$

$$\boldsymbol{t}_i = \boldsymbol{\omega}_{HO}\boldsymbol{h}_i \quad (8)$$

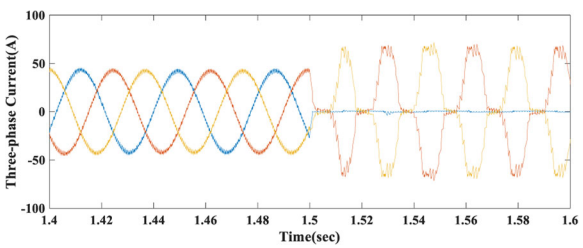

Fig. 4 The waveform when T_1 and T_4 are under open-circuit fault

Table 1 Labels of Different Fault Types

Fault Type	Label	Fault Type	Label
The Normal State	1	T_1&T_6 Open-circuit	12
T_1 Open-circuit	2	T_2&T_3 Open-circuit	13
T_2 Open-circuit	3	T_2&T_4 Open-circuit	14
T_3 Open-circuit	4	T_2&T_5 Open-circuit	15
T_4 Open-circuit	5	T_2&T_6 Open-circuit	16
T_5 Open-circuit	6	T_3&T_4 Open-circuit	17
T_6 Open-circuit	7	T_3&T_5 Open-circuit	18
T_1&T_2 Open-circuit	8	T_3&T_6 Open-circuit	19
T_1&T_3 Open-circuit	9	T_4&T_5 Open-circuit	20
T_1&T_4 Open-circuit	10	T_4&T_6 Open-circuit	21
T_1&T_5 Open-circuit	11	T_5&T_6 Open-circuit	22

In (7) and (8), $\boldsymbol{\omega_{HO}}$ is a $N \times K$ vector indicting the weights between the hidden layers and output layers, and $\boldsymbol{\omega_{IH}}$ is a $J \times N$ vector indicting the weights between the input layers and hidden layers, where N is the number of hidden nodes. $\boldsymbol{h}_i$ is the hidden layer's output vector and g is the activation function in hidden nodes [27].

Unlike general network, ELM generates values of $\boldsymbol{\omega_{IH}}$ randomly. By doing so, the learning speed of ELM network can be thousands times faster than the traditional methods using iterative algorithm.

3.2 Training process of ELM

To describe the training process of ELM, it can be divided into six phases as follows:

1) Divide data into training dataset and testing dataset.
2) Define the number of hidden neurons N and activation function g in hidden neurons.

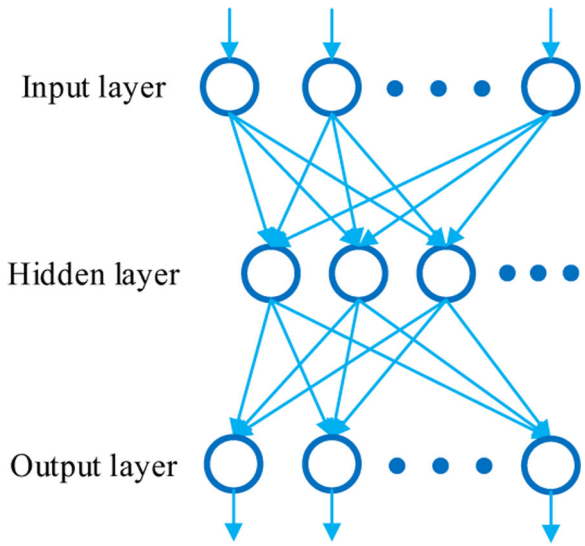

Fig. 5 Structure of ELM

3) Generate weights $\boldsymbol{\omega_{IH}}$ randomly within the range from 0 to 1.
4) Calculate the outputs of hidden nodes using (9), where x_j is the sample in training dataset and h_n compose hidden nodes output vectors $\boldsymbol{h}_i$ as:

$$h_n = g\left(\sum_{j=1}^{J} \omega_{jn} x_j\right) \tag{9}$$

5) Use Moore-Penrose pseudo inverse $\boldsymbol{\omega_{HO}}=\boldsymbol{H}^{-1}\boldsymbol{d}_i$ to obtain $\boldsymbol{\omega_{HO}}$, where $\boldsymbol{H}$ is the matrix consisting of $\boldsymbol{h}_i$.
6) Obtain actual output vector $\boldsymbol{t}_i$ and compare $\boldsymbol{t}_i$ with desired output $\boldsymbol{d}_i$, to calculate the accuracy of the training process.

For this study, to implement open-circuit fault diagnosis, ELM is applied to a multiclass classification. For the binary classification, the output function can be written as:

$$f_N(\boldsymbol{x}) = \text{sign}(\mathbf{H}(\boldsymbol{x})\beta) \tag{10}$$

where f_N indicates the final output of ELM. $\mathbf{H}$ is a feature mapping, converting input space with J-dimension to N-dimension hidden-layer space. In the binary case, only one node is included in the output layer and the final decision is based on which class label is closer to the output value. To fit in multi-classification, binary case can be modified into two solutions:

1) ***Multi-classification with Single Output***: In this case, the solution is similar to binary classification problem. The predicted class label of a given testing sample is closest to the output of ELM. The decision function needs to be modified by:

$$f_N(x) = \text{sign}\left(\mathbf{h}(\boldsymbol{x})\mathbf{H}^T\left(\frac{\mathbf{I}}{C} + \mathbf{H}\mathbf{H}^T\right)^{-1}\mathbf{T}\right) \tag{11}$$

where $\mathbf{h}$ denotes the output vector of the hidden layer corresponding to the input vector $\boldsymbol{x}$, $\mathbf{I}$ denotes an identity matrix and C is a regularization factor which can be defined by user depended on classification application.

2) ***Multi-classification with Multi-outputs***: For this multiclass case, the *number* of output nodes equals to the number of class labels. The predicted class label of a testing sample is the index number of the output node which has the highest output value. The decision mechanism is written as:

$$\text{label}(\boldsymbol{x}) = \arg \max_{i\in\{1,2,\ldots,m\}} f_i(\boldsymbol{x}) \tag{12}$$

where m denotes the total number of class labels, and $f_i(\boldsymbol{x})$ refers to the output function of the i^{th} output node, which forms the ELM classifier output set as $f(\boldsymbol{x}) = [f_1(\boldsymbol{x}),\ldots, f_m(\boldsymbol{x})]$.

In this IGBT open-circuit fault diagnosis, ELM is converted to the multi-classification with multi-outputs mode, with m equals to 22. Instead of iterative calculation in conventional SLFN, ELM randomly assigns input weights and thus releases the burden of lengthy calculation. By doing this, the training speed of ELM can be much faster than that of a conventional SLFN. Therefore, ELM greatly simplifies the learning process and becomes a practical algorithm in industrial applications [31] [32].

4 ELM-based ensemble classifier

Previous studies of ELM have focused on both regression and classification problems. ELM shows performance of high learning-speed and strong generalization capacity. However, during ELM training process, the input layer weight $\boldsymbol{\omega}_{IH}$, is generated randomly. Due to the stochastic value, ELM always suffers from inadequate consistency and stabilization [32]. To increase the accuracy, this paper designs an ensemble learning process.

4.1 Ensemble classifier principle

In the study of data analytic, ensemble learning is a methodology to compensate the results of each single classifier by utilizing diversity. It can reduce aggregated variance and tend to increase accuracy over the individuals [33].

Thus, an ensemble classifier of ELM is developed in this paper. First, the classifier structure consisting of a large quantity (200 in this case) of single ELM classifiers is defined. Based on the analysis above, for the same input data, the 200 ELM classifiers are unlikely to obtain the same outputs due to randomness. Each single ELM is trained to find out the mapping relationship between current and fault label and output weights will be achieved for each single ELM. Thus, the principle of ensemble classifier is to combine results and apply an evaluation process to determine the final classification, with a strategically designed decision-making mechanism.

4.2 Ensemble classifier structure

The structure of ELM ensemble classifier is depicted in Fig. 6. As shown, after the training process, the training features can be decided in individual ELM classifier, such as the output weights. Then the well trained ELM classifiers are clustered as an ensemble model.

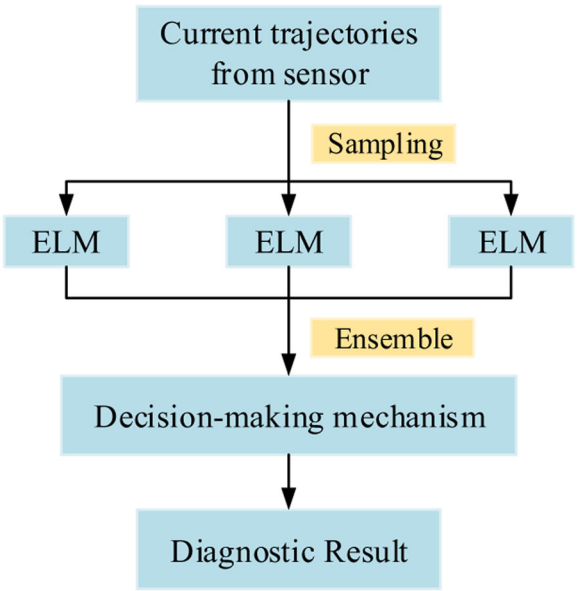

Fig. 6 Structure of Ensemble ELM Classifier

Based on the operating data in real-time, the proposed ensemble classifier is applied online for fault diagnosis. Using the decision-making mechanism, the final diagnosis output can be selected among individual ELM classifiers [30]. In addition, unlike traditional SLFN with long training time, ELM has high learning speed, and therefore, the proposed ensemble model is efficient.

In the testing process, each single ELM has its output $\boldsymbol{t}$ as $\boldsymbol{t} = [t_1,\ldots,t_J]$, where J is the number of output features. Assuming the total number of single ELM is p, a series of output $\boldsymbol{T}$ can be achieved as

$$\mathbf{T} = \begin{bmatrix} \mathbf{t}_1 \\ \vdots \\ \mathbf{t}_p \end{bmatrix} = \begin{bmatrix} t_{11} & \cdots & t_{1J} \\ \vdots & \ddots & \vdots \\ t_{p1} & \cdots & t_{pJ} \end{bmatrix} \tag{13}$$

For each column in (13), it represents the output results of each feature. The voting process is to choose the value with the most frequent occurrence in every column. Then a $1 \times J$ output vector, where each element is the most common value of each feature, can be obtained by:

$$y_j = \underset{i\in\{1,2,\ldots,p\}}{\text{mode}} \{t_{ij}\} \tag{14}$$

where y_j is the final result of the j^{th} instance, "mode" is the mathematical function for finding the mode of this sub-output set $\{t_{ij}\}$. Unlike errors existing in single ELM classification, this ensemble scheme minimizes the error as much as possible and the classification output is credible and reliable.

4.3 Diagnostic time window selection

In the training process described above, every input data can be expressed as $\boldsymbol{x} = [x_1,\ldots,x_D]$ with D features, where D is also called dimension. With higher dimension, diagnosis can achieve a higher accuracy with more learning time.

In the process of sampling, an exact length of waveform in time domain, namely time window, is selected. When the window width is not enough, information of fault signal cannot be fully achieved, leading to inadequate learning process, and resulting in errors in diagnostic system. On the other hand, when the window width is too large, although diagnostic accuracy is able to be guaranteed, the burden of learning process is increased and efficiency is low due to the lengthy learning time. Considering of applying to real-time online process, to keep balance between the cost of time and diagnostic accuracy is important. Therefore, to select appropriate time window width for fault diagnosis is an important task in testing process. In this study, diagnostic time window selection is equivalent to finding the appropriate sampling length of training data.

Fig. 7 illustrates a part of sampled waveform. In this figure, the horizontal axis represents the number of sampling point, which is also the time window width in this study. As seen, when the sampling number is 100, the sampled waveform is less than 1/4 periods, and does not provide reliable data for diagnosis. However, when the time window width reaches 400 or 500, the sampled waveform forms a period, and contains adequate information of the three-phase currents. On the other hand, if the sampling window width increases further, the information will be redundant and under this circumstance, the learning process will consist of lengthy calculation with reduced efficiency. By adjusting the sampling length, the diagnostic performance will achieve a trade-off between accuracy and learning burden.

5 Simulation validation

To verify the proposed data-driven based fault diagnosis method, a comprehensive and informative database is the fundamental requirement. In order to generate the database, a three-phase PWM voltage source inverter based induction motor drive system is simulated.

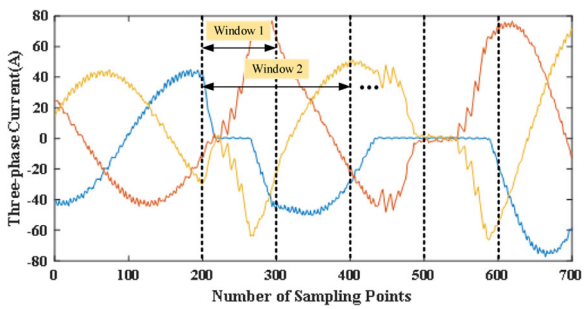

Fig. 7 The waveform when T_1 and T_4 are under open-circuit fault

5.1 Database generation

The simulation model of the drive system is implemented using MATLAB/Simulink software. The parameters of the simulation model are given in Table. 2. The simulation takes voltage ripple, harmonics, and speed and load fluctuations into consideration to verify the accuracy of the proposed diagnosis method under different fault states. Operation data are collected under different working states, including the injection of 100 Hz ripple voltage in the DC-link with amplitude varied from 1 to 100 V at 1 V interval, reference speed varied from 1 to 100 rad/s at 1 rad/s interval, and reference load torque varied from 21 to 120 N·m at 1 N·m interval. The sampling frequency is 10 kHz and the database is summarized in Table 3.

For 22 types of labels, 6600 sets of data can be obtained in the simulation model. To validate the single ELM classifier, those datasets are divided into two parts with 80% for training and 20% for testing, 5280 datasets for training and 1320 datasets for testing.

5.2 Parameter selection

Given different activation function searching patterns and neuron nodes, the performance comparison of ELM settings is analyzed in order to select optimal training parameters. To decide the relationship between single learner parameters and accuracy, the test accuracy A can be defined as:

$$A = \frac{(N-M)}{N} \times 100\% \tag{15}$$

where N is the total number of instances in test dataset, M is the number of misclassified datasets. To seek the optimal parameters, five types of activation function, i.e. triangular basis (Tribas), radial basis (Radbas), sign

Table 2 Parameters of the drive system

Comment	Value
DC-link voltage U_{dc}	700 V
Stator resistance R_s	0.435 Ω
Stator leakage inductance L_{ls}	4 mH
Rotor resistance R_r	0.816 Ω
Rotor leakage inductance L_{lr}	2 mH
Mutual inductance L_m	69.31 mH
Rated speed n_{rate}	2000(r/min)
Rated output power P_{rate}	11 kW
Number of the pole pairs	2

Table 3 Data acquisition

Simulation data	
DC-link ripple voltage	100 (1:100/1 V)
Reference speed	100 (1:100/1 rad/s)
Reference load torque	100 (21:120/1 N·m)
Open-circuit fault	2100

function (Sig), sine (Sin), and hard-limit (Hardlim) are compared in terms of optimal classification performance, in order to decide the optimal hidden node range for single classifier. The classification performance is shown in Fig. 8:

Fig. 8 shows that the sign activation function outperforms than the other four initial activation functions. Meanwhile, the trends of the curves indicate that increase of neuron nodes gradually increases the accuracy and in certain range, the accuracy is stable. As seen from Fig. 8, in the range from 1500 to 2000 using sign function, the accuracy of individual ELM classifier can be assured.

5.3 Time window selection

In this study, the simulation data is a 6600×1800 matrix, where 6600 refers to the number of datasets and 1800 indicates the number of data features in the time domain fault data. Every 600 features indicate the current data of each phase. For 10 kHz sampling frequency used in the simulation, every 100 data features correspond to a time window of 10 ms. Hence, the maximum time window in this study is 60 ms. When the length of sampling signal (i.e. time window width) varies from 10 ms to 60 ms at the interval of 10 ms, the classification performance is summarized in Fig. 9.

According to Fig. 9, increase the window width increases the testing accuracy. When the window width is short, e.g. 10 ms, classification accuracy is relative low due to inadequate learning. Meanwhile, when the time window width reaches a certain value, the accuracy stays

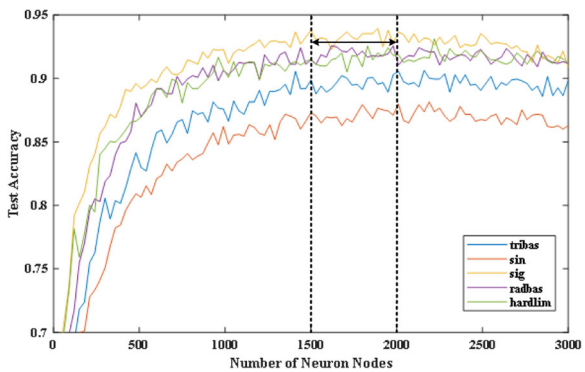

Fig. 8 Performance of single ELM classifier with different types of activation function

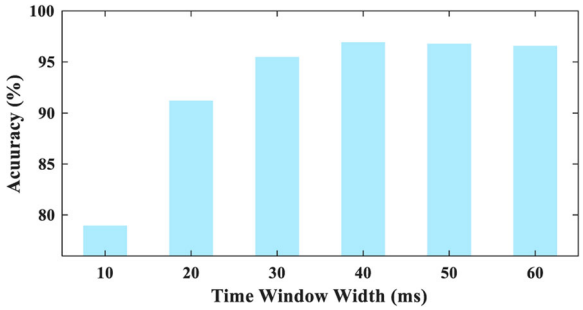

Fig. 9 Performance of ensemble ELM classifier with different time window width

high and becomes stable. Thus, in this case, 40 ms is determined as the optimal time window width, which guarantees the high accuracy with acceptable learning time.

5.4 Diagnosis results analysis and discussion

To show performance of ELM classifier, several neural networks are applied to train the same data to be compared with ELM. The networks in the control group include Support Vector Machine (SVM), Decision Tree (DT) and Naïve Bayes (NB). The classification performances of such learning methods are summarized in Table 4.

Table 4 illustrates that the average learning time of ELM classifier is 2.711 s with 93.80% average accuracy. The results show that in addition to faster learning speed, single ELM also has a higher testing accuracy than any other methods. Therefore, the ensemble structure of ELM is more efficient with less learning time, when compared with traditional neural network methods.

6 Conclusion

This paper designs an ensemble-based randomized classifier to identify IGBT open-circuit faults in three-phase PWM converters. Considering both single and double IGBT faults, the output three-phase converter currents are measured using the simulation model, and faults are diagnosed by ELM. To compensate the inadequacy of single ELM classification, an ensemble structure is designed to increase accuracy by combining a number of single classifiers. Moreover, an optimal value of time window is adopted to balance the tradeoff between diagnostic accuracy and ELM learning burden. The

Table 4 Classification Performance

Network Type	Average Learning Time	Average Testing Accuracy
ELM	2.711 s	93.80%
SVM	16.927 s	92.29%
DT	5.366 s	90.01%
NB	5.221 s	68.18%

simulation shows that, compared with other traditional learning algorithms, ELM has better performance in both classification accuracy and learning time. This ensemble ELM structure can identify IGBT open-circuit faults with a much higher diagnosis accuracy of 96.89% in 40 ms. It also shows that the proposed data-driven scheme is independent of voltage ripple, harmonics, and speed and load fluctuations. Thus, the proposed scheme is efficient and reliable in practical applications.

Abbreviations

CHMLIS: Cascaded H-bridge multilevel inverter system; DT: Decision tree; ELM: Extreme learning machine; IGBT: Insulated gate bipolar transistor; NB: Naïve Bayes; PCA: Principle component analysis; PWM: Pulse width modulation; SLFN: Single hidden layer feed-forward neural network; SVD: Singular value decomposition; SVM: Support vector machine

Acknowledgements

Not applicable.

Funding

The authors declare that they have no funding.

Availability of data and materials

Please contact author for data requests.

Authors' contributions

Yang Xia conceived of the study, participated in its design, carried out the programing test and drafted the manuscript. Bin Gou generated the database and participated in the design of the study. Yan Xu participated in its design and coordination and helped to draft the manuscript. All authors read and approved the final manuscript.

Authors' information

Yang Xia received the B.E. degrees from Xi'an Jiaotong University, Xi'an, China, in 2017. He is currently working toward the M.E degree at Nanyang Technological University, Singapore.

Bin Gou received the B.S and Ph.D. degrees in electrical engineering from Southwest Jiaotong University, Chengdu, China, in 2010 and 2016, respectively. He is currently a Research Fellow in the School of Electrical and Electronic Engineering, Nanyang Technological University, Singapore.

Yan Xu received the B.E. and M.E. degrees from South China University of Technology, Guangzhou, China, in 2008 and 2011, respectively, and the Ph.D. degree from The University of Newcastle, Callaghan, N.S.W., Australia, in 2013. He is currently an Assistant Professor with a Nanyang Assistant Professorship in the School of Electrical and Electronic Engineering, Nanyang Technological University, Singapore.

Competing interests

The authors declare that they have no competing interests.

Received: 4 March 2018 Accepted: 11 October 2018
Published online: 06 November 2018

References

1. Ding, X., Du, M., Duan, C., Guo, H., Xiong, R., Xu, J., Cheng, J., & Luk, P. "analytical and experimental evaluation of SiC-inverter nonlinearities for traction drives used in electric vehicles," *IEEE Trans. Vehicular technology*, vol. 67, no. 1, pp. 146–159, Jan. 2018
2. Song, Y., & Wang, B. (2013). Survey on reliability of power electronic systems. *IEEE Trans Power electronics, 28*, 591–604.
3. B. Lu, and S. K. Sharma, "A literature review of IGBT fault diagnostic and protection methods for power inverters," IEEE trans. Industry application, vol. 45, pp. 1770–1777, SEP/OCT. 2009.
4. Li, B., Shi, S., Wang, B., Wang, G., Wang, W., & Xu, D. (2016). Fault diagnosis and tolerant control of single IGBT open-circuit failure in modular multilevel converters. *IEEE Trans. Power Electronics, 31*, 3165–3176.
5. Gao, Z., Cecati, C., & Ding, S. X. (2015). A survey of fault diagnosis and fault-tolerant techniques-part I: Fault diagnosis with model–based and signal-based approaches. *IEEE Trans. Industrial Electronics, 62*, 3757–3767.
6. Choi, U., Blaabjerg, F., & Lee, K. (2015). Study and handling methods of power module failures in power electronic converter systems. *IEEE Trans. Power Electronics, 30*, 2517–2533.
7. J. O.Estima, and A. J. Marques Cardoso. (2011). A new approach for real-time multiple open-circuit fault diagnosis in voltage-source inverters. In *IEEE trans. Industry application, vol. 47, pp. 2487–2494, NOV/DEC*.
8. Youssef, A. B., Khil, S. K. E., & Slama-Belkhodja, I. (2013). State observer-based sensor fault detection and isolation, and fault tolerant control of a single-phase PWM rectifier for electric railway traction. *IEEE Trans. Power Electronics, 28*, 5842–5853.
9. Khwan-on, S., de Lillo, L., Empringham, L., & Wheeler, P. (2012). Fault-tolerant matrix converter motor drives with fault detection of open switch faults. *IEEE Trans Industrial electronics, 59*, 257–268.
10. Lamb, J., & Mirafzal, B. (2017). Open-circuit IGBT fault detection and location isolation for cascaded multilevel converters. *IEEE Trans. Industrial electronics, 64*, 4846–4856.
11. Nie, S., Pei, X., Chen, Y., & Kang, Y. (2014). Fault diagnosis of PWM DC-DC converters based on magnetic component voltages equation. *IEEE Trans. Power Electronics, 29*, 4978–4988.
12. Gou, B., Ge, X., Wang, S., Feng, X., Kuo, J. B., & Habetler, T. G. (2016). An open-switch fault diagnosis method for single-phase PWM rectifier using a model-based approach in high-speed railway electrical traction drive system. *IEEE Trans. Power Electronics, 31*, 3816–3826.
13. Sheng, H., Wang, F., & Tipton IV, C. W. (2012). A fault detection and protection scheme for three-level DC-DC converters based on monitoring flying capacitor voltage. *IEEE Trans Power Electronics, 27*, 685–697.
14. Estima, J. O., & Cardoso, A. J. M. (2013). A new algorithm for real-time multiple open-circuit fault diagnosis in voltage-fed PWM motor drives by the reference current errors. *IEEE Trans. Industrial electronics, 60*, 3496–3505.
15. Sleszynski, W., Nieznanski, J., & Cichowski, A. (2009). Open-transistor fault diagnostics in voltage-source inverters by analyzing the load currents. *IEEE Trans. Industrial electronics, 56*, 4681–4688.
16. Freire, N. M. A., Estima, J. O., & Cardoso, A. J. M. (2013). Open-circuit fault diagnosis in PMSG drives for wind turbine applications. *IEEE Trans. Industrial electronics, 60*, 3957–3967.
17. Zhang, R., Xu, Y., Dong, Z. Y., & Hill, D. J. (2012). Feature selection for intelligent stability assessment of power systems. *Proc. Power & Energy Society General Meeting*, 1–7.
18. Wang, T., Xu, H., Han, J., Elbouchikhi, E., & Benbouzid, M. E. H. (s2015). Cascaded H-bridge multilevel inverter system fault diagnosis using a PCA and multiclass relevance vector machine approach. *IEEE Trans. Power Electronics, 30*, 7006–7018.
19. Foo, G. H. B., Zhang, X., & Vilathgamuwa, D. M. (2013). A sensor fault detection and isolation method interior permanent-magnet synchronous motor drives based on an extended Kalman filter. *IEEE Trans Industrial Electronics, 60*, 3485–3495.
20. Cho, H. C., Knowles, J., Fadali, M. S., & Lee, K. S. (2010). " Fault detection and isolation of induction motors using recurrent neural networks and dynamic Bayesian modeling" IEEE Trans. *Control system technology, 18*, 430–437.
21. Khomfoi, S., & Tolbert, L. (2007). Fault diagnosis system for a multilevel inverter using a neural network. *IEEE Trans. Power Electronics, 22*, 1062–1069.
22. Zidani, F., Diallo, D., Benbouzid, M. E. H., & Naït-Saïd, R. (2008). A fuzzy-based approach for the diagnosis of fault modes in a voltage-fed PWM inverter induction motor drive. *IEEE Trans. Industrial Electronics, 55*, 586–593.
23. Han, R., & Zhou, Q. (2016). Data-driven solutions for power system fault analysis and novelty detection. *Proc The 11th International Conference on Computer Science & Education*, 86–91.
24. C. Huang, J. Zhao, and C. Wu, "Data-based inverter IGBT open-circuit fault diagnosis in vector control induction motor drives," in Proc. IEEE 8th Conference on Industrial Electronics and Application, pp. 1039–1044 2013.
25. Cai, B., Zhao, Y., Liu, H., & Xie, M. (2017). A data-driven fault diagnosis methodology in three-phase inverters for PMSM drive systems. *IEEE Trans. Power Electronics, 32*, 5590–5600.
26. Gao, Z., Cecati, C., & Ding, S. X. (2015). "A survey of fault diagnosis and fault-tolerant techniques-part II: Fault diagnosis with knowledge–based and hybrid/active approaches," *IEEE Trans. Industrial. Electronics, 62*, 3768–3774.
27. Huang, G. B., Zhu, Q. Y., & Siew, C. K. (2006). Extreme learning machine: Theory and applications. *Neurocomputing, 70*, 489–501.

28. A. Khamis, Y. Xu, Z. Y. Dong, and R. Zhang, "Faster detection of microgrid islanding events using an adaptive ensemble classifier," IEEE Trans. Smart Grid, vol. 9, pp. 1889–1899, AUG. 2016.
29. Y. Xu, Z. Y. Dong, J. H. Zhao, P. Zhang, and K. P. Wong, "A reliable intelligent system for real-time dynamic security assessment of power system," IEEE Trans. Power System, vol. 27, pp. 1253–1263, AUG. 2012.
30. Pei, X., Nie, S., Chen, Y., & Kang, Y. (2012). Open-circuit fault diagnosis and fault-tolerant strategies for full-bridge DC-DC converters. *IEEE Trans. Power Electronics, 27*, 2550–2565.
31. Huang, G. B., & Chen, L. (2008). Enhanced random search based incremental extreme learning machine. *Neurocomputing, 71*, 3460–3468.
32. Huang, G., & Huang, G. B. (2015). Trends in extreme learning machine: A review. *Neural Netw, 61*, 32–48.
33. Y. Zhang, Y. Xu, Z. Y. Dong, Z. Xu and, K. P. Wong, "Intelligent early warning of power system dynamic insecurity risk: Toward optimal accuracy-earliness tradeoff," IEEE Trans Industrial informatics, vol. 13, pp. 2544–2554, OCT. 2017.